This article has been accepted for publication in IEEE Access. This is the author's version which has not been fully edited and content may change prior to final publication. Citation information: DOI 10.1109/ACCESS.2022.3195040

IEEE Access
Multidisciplinary | Rapid Review | Open Access Journal

Date of publication xxxx 00, 0000, date of current version xxxx 00, 0000.

*Digital Object Identifier 10.1109/ACCESS.2022.DOI*

# A Fractionally Asymmetric Sub–Nyquist Baseband Receiver Design and Implementation for Phase Modulated Signals

**ZEYNEP GÜRKAŞ-AYDIN[1] (Member, IEEE) and SERHAN YARKAN[2] (Senior Member, IEEE)**
[1]Department of Computer Engineering, Istanbul University - Cerrahpasa, Istanbul, TURKEY (e-mail: zeynepg@iuc.edu.tr)
[2]Department of Electric-Electronics Engineering, Istanbul Commerce University, Istanbul, TURKEY (e-mail: syarkan@ticaret.edu.tr)

Corresponding author: Zeynep GÜRKAŞ-AYDIN (e-mail: zeynepg@iuc.edu.tr).

**ABSTRACT** Sub–Nyquist sampling is a technique which has various applications in signal processing and communication technologies. Memory relaxation, peripherals operating at relatively lower speeds, and consequently low–power consumption designs are prominent motivations in sub–Nyquist receiver studies. Although these motivations seem to be attractive, instability and information loss are major drawbacks of sub–Nyquist approaches in comparison with Nyquist–Shannon sampling applications. Nevertheless, sub-Nyquist receivers could still provide several ways of recovering information to some extent in case they are fortified with appropriate interpolation mechanisms. Hence, this study proposes a fractionally asymmetric sub–Nyquist baseband receiver design for phase modulation (PM) signal reception. The proposed method takes advantage of statistical behaviors of the received signal passing through physical propagation medium and adopts an autoregressive process to recover the phase information required. The proposed design is implemented on a software-defined radio (SDR) platform operating in near real–time and tested in a real–world communication environment. Results and discussions are provided along with the future directions.

**INDEX TERMS** baseband communication, digital signal processor, software-defined radio, subsampling

## I. INTRODUCTION

ALONG with the relentless advances in digital technology, wireless communication systems have permeated the modern civilization and have become an integral part of it. Recent predictions report that there will be approximately 30 billion devices connected in addition to 6 billion overall global mobile subscribers by 2023 [1]. In parallel with such an ever–increasing demand and push, prominent industries such as health, commerce, agriculture, education, logistics, and transportation experience dramatic shifts in paradigms driven by the wireless revolution. It is believed that ubiquitous connectivity, cyber–physical systems, smart cities, intelligent transport systems (ITS), green environments, Internet of things (IoT), and software–defined metasurfaces will be the key concepts in the near future with the aid of machine learning applications and services [2]–[6].

It is clear that deployment of any next generation system envisioned above should be able to find a place for itself in the overcrowded electromagnetic spectrum (EM) and co–exist with already–present technologies. Furthermore, it should follow critical design principles such as being parsimonious with size, power consumption, computational complexity, and cost; however, providing utmost performance along with several other parameters. From the practical point of view, one could claim that almost all of the principles and/or parameters listed above conflict with each other one way or another. One of the plausible strategies to overcome such conflicts is to sustain certain quality of service (QoS) requirements rather than to impose utmost performance with –relatively– low resources or support. Of course, conflicting requirements pave the way of reaching a compromise between several parameters. From this perspective, optimization could only be achieved when specific problems are tackled by specific designs and implementations [7], [8].

Sub–Nyquist receivers are prominent examples of the aforementioned parsimonious designs in many aspects. They are employed in many areas and used in many applications in the literature including ranging, localization, spectrum



This work is licensed under a Creative Commons Attribution 4.0 License. For more information, see https://creativecommons.org/licenses/by/4.0/

This article has been accepted for publication in IEEE Access. This is the author's version which has not been fully edited and
content may change prior to final publication. Citation information: DOI 10.1109/ACCESS.2022.3195040



sensing, signal identification, and even communications applications [9]–[14]. Any sub–Nyquist approach relies on two fundamental properties: $K$–sparsity, which is based on a complete description of the signal of interest in terms of orthogonal projection (with $K$ non–zero entries) and coherence [15]–[17]. This perspective brings about an important concept called information rate [18]. It is known that information rate of many signals (generated either by natural or synthetic processes) is less than their physical bandwidth. Furthermore, some approaches as in machine learning– and artificial intelligence–based designs are solely concerned with so–called "feature rate" and not even with information rate [19]. Finally, it must be stated that there is a significant effort in design and implementation of sub–Nyquist receiver structures and their applications in emerging technologies such as IoT [20]–[23, and references therein]. In contrast, there are a few studies present in the literature specifically focusing on receivers based on sub–Nyquist sampling without considering the channel impairments [24]. Therefore, in this study, a fractionally asymmetric sub–Nyquist receiver is proposed, designed, implemented, and tested in a physical environment. Having said that, as can be seen from the presented studies in the literature, to the best knowledge of authors', there exists no fractionally asymmetric sub–Nyquist receiver design. Furthermore, the present designs are application–specific, which end up having a relatively narrower scope in terms of both being applicable to analog and digital systems together. In this regard, it is worth mentioning that this study differs from the studies in the literature in the following two prominent ways: First, the proposed design does not focus on a single, special case, namely symmetric sub–Nyquist sampling. It considers asymmetric sub–Nyquist receiver structure as the generalization of sub–Nyquist approaches by relying on the impact of propagation medium on the transmit signal. Second, this study does not rely on higher–order statistics and/or transform domain techniques. In this regard, the contributions of this study are the following: (i) A fractionally asymmetric sub–Nyquist receiver that is fortified with plain, linear interpolation–based method (in contrast to some non–linear methods employed in the literature) is employed to restore the phase information presumably lost in sub–Nyquist operation, and (ii) it is demonstrated that such a receiver could still compensate for the information loss to some extent and perform satisfactorily under real–world conditions. The rest of the paper is organized as follows: Section II introduces the signal and system model along with the fundamental assumptions. Section III outlines the proposed method in detail. Data collection procedures, relevant details, results and their interpretations are discussed in Section V and in Section VI, respectively. Finally, Section VII provides the closing remarks along with future directions.

## II. SIGNAL AND SYSTEM MODELS

In this section, both signal and system models are introduced along with fundamental assumptions for a generic wireless communications scenario. Key points are provided and highlighted for the upcoming sections and subsections as well.

### A. SIGNAL MODEL

A general linear, time–varying complex baseband channel impulse response is given by:

$$h(t,\tau) = \sum_{k=1}^{N} a_k(t)\delta\left(t-\tau_k(t)\right) e^{j\left(2\pi f_k^D(t)+\theta_k(t)\right)} \tag{1}$$

where $N$ is the number of resolvable multipath components; $a_k(\cdot)$ is the magnitude of $k$–th component; $\delta(\cdot)$ is the Dirac delta function; $\tau_k(\cdot)$ is the $k$–th delay; $f_k^D(\cdot)$ and $\theta_k(\cdot)$ are Doppler shift and phase offset experienced by the corresponding $k$–th multipath component, respectively, and $j=\sqrt{-1}$. Depending on the scenario, a further extension is possible by considering:

$$a_k(t)e^{j\left(2\pi f_k^D(t)+\theta_k(t)\right)} = s_k(t)+d_k(t) \tag{2}$$

as major contribution of the power is obtained by the specular component, $s_k(t)$, along with a relatively weaker contribution of a diffused component, $d_k(t)$. This way, the receiver, if possible, could be designed based on the perspective given in (2). This representation paves also way of arranging resolvable multipath components via certain parameters according to the communication scenario to be considered for various purposes.

Given $h(t,\tau)$, the received signal at baseband is generally expressed in the form of:

$$r(t) = x(t) \circledast h(t,\tau) + \omega(t) \tag{3}$$

where $x(t)$ is the transmitted signal at baseband; $\circledast$ denotes the convolution operator; $\omega(t)$ is the complex baseband additive white Gaussian noise (AWGN) term consisting of both in–phase and quadrature components, $\omega_I(t)$ and $\omega_Q(t)$, respectively, where each component is $\mathcal{N}\left(0,\sigma_\omega^2/2\right)$. Without loss of generality, channel statistics are assumed to be stationary (in any sense) for a sufficiently long period of time. Furthermore, in order to have a more tractable analysis, (3) is assumed to be of the following form:

$$r(t) = x(t) \circledast h(t) + \omega(t) \tag{4}$$

where the channel, $h(t)$, acts a linear, time–invariant filter.

### B. SYSTEM MODEL

Depending on the scenario, receiver is considered to be a monolithic statistical decision mechanism such that its input values are translated into a set of output values under certain rules and conditions. From this point of view, receiver could be subdivided into further blocks in such a way that complex baseband equivalent in–phase/quadrature (I/Q) signal is pre–processed and then prepared for further stages. In this regard, system model includes all the relevant modules at the receiver side such that the passband received signal



This work is licensed under a Creative Commons Attribution 4.0 License. For more information, see https://creativecommons.org/licenses/by/4.0/

This article has been accepted for publication in IEEE Access. This is the author's version which has not been fully edited and
content may change prior to final publication. Citation information: DOI 10.1109/ACCESS.2022.3195040



is translated into complex baseband equivalent I/Q signal which is given in (3) encompassing all sets of impairments. A complete set of blocks involved in a generic analog front–end receiver is given in Figure 1.

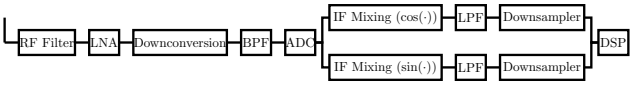


**Figure 1.** A generic analog front–end receiver followed by a digital baseband DSP.

For the given system block structure, complex baseband equivalent signal is received and discretized satisfying Nyquist criterion under flat–fading assumption as:

$$r[n] = x[n] \circledast h[n] + \omega[n] \tag{5}$$

Considering the discrete–time convolution operation:

$$r[n] = \sum_{k=-\infty}^{\infty} x[k]h[n-k] + \omega[n] \tag{6}$$

where

$$h[n] = \sum_{p=0}^{L-1} \alpha_p \operatorname{sinc}(n - \tau_p B) \tag{7}$$

with $B$ is the anti–alias filter bandwidth satisfying Nyquist criterion;

$$\alpha_p = a_p(p/B)e^{j\left(2\pi f_p^D (p/B) + \theta_p(p/B)\right)} \tag{8}$$

could be written where $\operatorname{sinc}(\cdot)$ is the normalized cardinal sine function, and $a_p$ is the gain affiliated with the $p$–th term.

Once the received signal is discretized in accordance with (6) and (7), it can be re–written as $r[n] = r_I[n] + jr_Q[n]$ where $r_I[n]$ and $r_Q[n]$ are the $n$–th sample of the in–phase and quadrature components of the discrete–time version of the received signal.

## III. PROPOSED METHOD

### A. THE PROBLEM STATEMENT

Specifically, the transmit signal, $x_{\text{pb}}(t)$, could be written as a general constant–envelope phase modulation (PM) passband signal:

$$x_{\text{pb}}(t) = A_c \cos(2\pi f_c t + k_p m(t)) \tag{9}$$

where $A_c$ represents the constant peak value of the harmonic; $f_c$ is the transmit frequency; $k_p$ is the frequency deviation constant; and $m(t)$ is a specific form of a message signal at baseband depending on the choice of phase or frequency modulation. Considering the complex baseband equivalent representation under coherent reception:

$$x(t) = \frac{A_c}{2}\left(\cos(k_p m(t)) + j\sin(k_p m(t))\right) \tag{10}$$

is obtained in conjunction with (3).

In this regard, research problem could be stated as follows. Is it possible to demodulate a general PM signal with the use of asymmetrically fractional sub–Nyquist sampling baseband receiver? What would be the performance of such a receiver?

### B. SUB–NYQUIST RECEIVER SCHEME

A sub–Nyquist receiver buffers a stream of incoming samples, $r[n]$, as a two–dimensional array where, at first, both real and imaginary components of $r[n]$ are aligned.[1] Next, the receiver forms a fractionally "asymmetric" sub–list of components as a special subset of discrete multi-coset sampling process [25] with:

$$\hat{r}[n] = r_I[K(n-1) + \Delta] + jr_Q[Kn] \tag{11}$$

where $K, \Delta \in \mathbb{Z}^+$. Here, $\Delta$ denotes the parameter that preserves the intentional asymmetry with the case $\Delta \neq K$. It is clear that the case $1 < \Delta = K$ reduces down to regular, "symmetric" downsampling operation. With the use of both $K$ and $\Delta$ along with appropriate configurations, $\hat{r}[n]$ carries asymmetric index pairs of I/Q branches of $r[n]$. Moreover, the sampling rate is intentionally reduced by a factor of $K$. At this point, one could elaborate more on the relationship between $\Delta$ and $K$ along with its implications on the asymmetrically subsampled signal. As stated before, in order to distinguish asymmetric subsampling from regular downsampling, the condition $\Delta \neq K$ should be satisfied. Once the sumbsapling rate $K$ is decided, intentional assymmetry between indices of $r_I[\cdot]$ and $r_Q[\cdot]$ could only be achieved by assigning $\Delta$ values from $G_\Delta\{0, 1, \cdots, K-1\}$. Evidently, the values of $\Delta \in G_\Delta$ somehow acts as a parameter which controls the separation of I/Q samples in time and eventually the correlation between them while keeping the downsampling rate at $K$ and preserving the intentional asymmetry between the samples of I/Q branches. In order to see this behavior, first, assume that $\Delta = 0$. This case, statistically speaking, leads to the least possible correlation between corresponding samples of I/Q branches, since $\Delta = 0$ yields the greatest possible time separation between I/Q branches among all possible configurations. In other words, $\Delta = 0$ yields $r_I[Kn - K]$ and $r_Q[Kn]$, hence; in this regime, $r_I[\cdot]$ lags always $K$ samples behind $r_Q[\cdot]$ and statistically speaking, the correlation of the asymmetrically subsampled signal reaches its minimum as compared to that in the regular, downsampled version. In contrast, $\Delta = K - 1$ leads to statistically the highest possible correlation between corresponding samples of I/Q branches, since $\Delta = K - 1$ yields the lowest possible time separation between I/Q branches among all possible configurations. More specifically, $\Delta = K - 1$ produces $r_I[Kn - 1]$ and $r_Q[Kn]$, hence; in such a scheme, $r_I[\cdot]$ lags always one sample behind $r_Q[\cdot]$ and statistically speaking, the correlation of the asymmetrically subsampled signal reaches its maximum as compared to that in the regular, downsampled version.

[1]Here, the buffer design such as linear or circular is excluded in the analysis since it is outside the scope of this study. However, the design choice might affect the hardware performance; therefore, a detailed further investigation is required.



This work is licensed under a Creative Commons Attribution 4.0 License. For more information, see https://creativecommons.org/licenses/by/4.0/

This article has been accepted for publication in IEEE Access. This is the author's version which has not been fully edited and
content may change prior to final publication. Citation information: DOI 10.1109/ACCESS.2022.3195040



For the sake of simplicity, the asymmetry parameter will hereinafter be assumed to be unity, $\Delta = 1$, which provides a performance analysis that is very close to the worst–case scenario in terms of statistical correlations, while not affecting the analysis methodology and design itself. Thus, the complex baseband version of the received signal passed through the channel is given by:

$$\begin{aligned}\hat{r}[n] = \\ &\frac{A_c}{2}\sum_{i=-\infty}^{\infty}\left(\sum_{u=0}^{L-1}\alpha_u \operatorname{sinc}\left(n-Ki-K+1-\tau_u B\right)\times\right.\\ &\cdot\cos\left(k_p m[Ki-K+1]\right)+\\ &\left.\cdot\, j\sum_{v=0}^{L-1}\alpha_v \operatorname{sinc}\left(n-Ki-\tau_v B\right)\sin\left(k_p m[Ki]\right)\right)\end{aligned} \tag{12}$$

In order to ease the representation, let $k_p m[Ki-K+1] = \psi_m[i]$ and $k_p m[Ki] = \varphi_m[i]$ where both $\psi_m[i]$ and $\varphi_m[i]$ are assumed to manifest the characteristics of the message signal and possible effects of other impairments. Hence (13) could be restated as:

$$\begin{aligned}\hat{r}[n] = \frac{A_c}{2}\sum_{i=-\infty}^{\infty}\times\\ &\cdot\left(\sum_{u=0}^{L-1}\alpha_u \operatorname{sinc}\left(n-Ki-K+1-\tau_u B\right)\cos\left(\psi_m[i]\right)+\right.\\ &\left.\cdot\, j\sum_{v=0}^{L-1}\alpha_v \operatorname{sinc}\left(n-Ki-\tau_v B\right)\sin\left(\varphi_m[i]\right)\right)\end{aligned} \tag{13}$$

In light of the discussion above, assuming that the phase is striven to recover for PM signals on sample basis and considering the channel dynamics in time projected on cardinal sine, the proposed method employs the following approximation for demodulation purposes under zero–mean assumption:

$$\hat{r}[n] = \varrho\hat{r}[n-1] + \sqrt{1-\varrho^2}w[n] \tag{14}$$

where $\varrho$ is a constant and $w[\cdot]$ is the discrete–time complex AWGN of the form of the noise mentioned in (3). With the use of equation above, it will be shown that an asymmetrical fractionally sub–Nyquist sampled received signal could still recover the phase information to some extent under the assumptions discussed in detail above.

### 1) Baseband Differentiator Discriminant Analysis for Frequency Modulation Signals

Well–known baseband differentiator for frequency modulation (FM) signals operating on a finite buffer of size of $M$, populated by baseband I/Q samples obtained under Nyquist criterion yields the following real–valued signal:

$$\theta[n] = \frac{r_I[n]\,\mathrm{D}\left\{r_Q[n]\right\} - r_Q[n]\,\mathrm{D}\left\{r_I[n]\right\}}{G\left(\left|\left(r_I[n]\right)\right|^2 + \left|\left(r_Q[n]\right)\right|^2\right)} \tag{15}$$

where $G$ is the normalization constant for appropriate unit and normalization conversion and $n$ denotes the memory indices of the streaming buffer $n = 0, 1, \cdots, M-1$. Note that in conjunction with sufficiently high sampling rates (still remaining below Nyquist) $\left|\left(r_I[n]\right)\right|^2 + \left|\left(r_Q[n]\right)\right|^2$ could be approximated with a constant especially when constant envelope signals are considered. Before proceeding with the details of such a simplification, it is noteworthy to discuss the characteristics of sufficiently high sampling rates while remaining below Nyquist rate. Especially for angle modulation techniques, it is known that physical bandwidth of signals diverge due to the nature of non–linear structure of the modulation operation. Furthermore, the communication channel introduces correlation into the transmit signal via several propagation mechanisms such as multipath reflection. Therefore, there is a distinction between physical bandwidth of a signal passed through a channel and its information bearing portion in its power spectrum, which is always less than its physical bandwidth. In this regard, sufficiently high sampling rates while residing below Nyquist limit corresponds to the scenarios where subsampling receiver could capture at least the information bearing portion of the power spectrum of the signal of interest. Depending on the application, there are studies in the literature which report that sampling rates could be reduced down to even less than 30% of the physical bandwidth of the signal of interest [26]–[28].Having said that, all continuous phase modulation signals whether the message signal being analog or digital could be written at the complex baseband in discrete–time as:

$$s[n] = A_s e^{\jmath\Theta[n]} = \left(s_I[n] + \jmath s_Q[n]\right) \tag{16}$$

where $A_s$ is the magnitude of the complex baseband signal; whereas $\Theta[n]$ is the phase trajectory of the message signal; and both $s_I[n]$ and $s_Q[n]$ are the in–phase and quadrature components of the signal, respectively. As can be inferred,

$$|s[n]|^2 = |s_I[n]|^2 + |s_Q[n]|^2 = A_s$$

is obtained. Therefore, the term $\left|\left(r_I[n]\right)\right|^2 + \left|\left(r_Q[n]\right)\right|^2$ in the denominator of (15) could be captured by a constant and one could express (15) as:

$$\hat{\theta}[n] = \kappa\left(r_I[n]\,\mathrm{D}\left\{r_Q[n]\right\} - r_Q[n]\,\mathrm{D}\left\{r_I[n]\right\}\right) \tag{17}$$

where $\kappa$ denotes the term that accommodates all constant–behavior parameters including the constant envelope attribute of the denominator of (15) . As can be seen, baseband discriminator includes the first–order difference operator, namely $\mathrm{D}\{\cdot\}$, acting on the discrete–time stochastic processes $r_{I,Q}[n]$. This brings about two important cases regarding the model based on the value of $\varrho$. In the first case, let $\varrho$ approach unity. Such a special scenario in the presence of first–order difference operator reduces down to random walk where phase information is considered to be pure white noise (possibly with a very low variance). From the practical point of view, this conclusion does not imply a



This work is licensed under a Creative Commons Attribution 4.0 License. For more information, see https://creativecommons.org/licenses/by/4.0/

This article has been accepted for publication in IEEE Access. This is the author's version which has not been fully edited and
content may change prior to final publication. Citation information: DOI 10.1109/ACCESS.2022.3195040



realistic model since information sources generally manifest coherence to some extent. Nevertheless, this case provides some insight into the performance boundaries of the model. In the second case, let $\varrho$ converge. Such a scenario leads to problems in the presence of $\mathrm{D}\{\cdot\}$ operator if the noise process is assumed to be white. On the other hand, in case noise process is assumed to satisfy properties of Wiener–Lévy process, then $\mathrm{D}\{\cdot\}$ implies a white noise process. As in the first case, such a boundary condition provides some insight into performance limitations of the model from the theoretical point of view. Therefore, it is expected that $\varrho$ could be regarded as a parameter whose value could capture many characteristics of the process considered for both the actual discrete–time random stochastic processes $r_{I,Q}[n]$ and their first–order differences.

Excluding the boundary cases for $\varrho$, it is clear that the difference operator leads to a new autoregressive process with the following expression:

$$\mathrm{D}\{r_{I,Q}[n]\} = (1-\varrho)\, r_{I,Q}[n-1] + \sqrt{1-\varrho^2} w_{I,Q}[n] \quad (18)$$

Thus, one could express the baseband phase estimation as:

$$\hat{\theta}[n] = \kappa \Big\{ (1-\varrho)\, r_I[n] r_Q[n-1] + \sqrt{1-\varrho^2} r_I[n] w_Q[n] - (1-\varrho)\, r_Q[n] r_I[n-1] - \sqrt{1-\varrho^2} r_Q[n] w_I[n] \Big\} \quad (19)$$

After reorganizing the terms in (19):

$$\hat{\theta}[n] = \kappa \Big\{ (1-\varrho)\,(r_I[n] r_Q[n-1] - r_Q[n] r_I[n-1]) + \cdot \sqrt{1-\varrho^2}\,(r_I[n] w_Q[n] - r_Q[n] w_I[n]) \Big\} \quad (20)$$

is obtained. As can be inferred, $\hat{\theta}[n]$ is a zero–mean signal in case no imbalance is present between in–phase and quadrature branches. The proposed method is summarized as a block diagram given in Figure 2 focusing solely on the baseband part. As can be seen from the figure, the proposed method incorporates the noise into the autoregressive process in a peculiar way such that both in–phase and quadrature components of the received signal samples weight both noise and the delayed version of the input.

### 2) Analysis of Flat–Fading Channel Scenario

In order to have a better grasp of the estimator, a generic communication scenario could be considered. Assuming that the process satisfies wide–sense stationary (WSS) assumptions within the buffer size of $M$, the following could be written as:

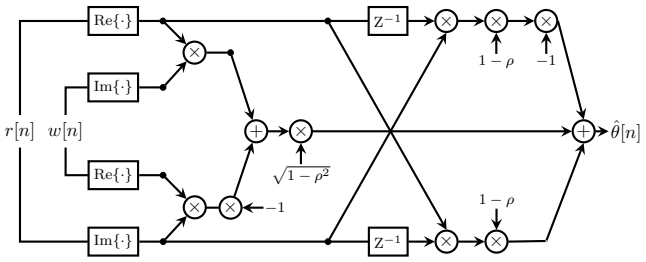


**Figure 2.** The block diagram of the proposed method at baseband. Here, the $\mathrm{Re}\{\cdot\}$, $\mathrm{Im}\{\cdot\}$, and $\mathrm{Z}^{-1}$ denote, real part of its input, imaginary part of its input, and the unit sample delay operator, respectively.

$$\begin{aligned} R_{\hat{\theta}}[k] &= E\left\{\hat{\theta}[n]\hat{\theta}[n+k]\right\}_{k>0} \\ &= \kappa^2 \Big\{ (1-\varrho) \times \\ &\cdot \Big\{ 2R_{r_I}[k]R_{r_Q}[k] - R_{r_I}[k+1]R_{r_Q}[k-1] - \\ &\cdot R_{r_I}[k-1]R_{r_Q}[k+1] \Big\} \Big\} \end{aligned} \quad (21)$$

For the sake of tractability, let $L=1$ and $\tau_u = \tau_v = 0$ as in a generic flat–fading scenario. Then,

$$\hat{r}[n] = \frac{A_c}{2} \sum_{i=-\infty}^{\infty} \mathrm{sinc}\,(n - i(k;I,Q)) \times \Big( \alpha_u \cos(\psi_m[i]) + j\alpha_v \sin(\varphi_m[i]) \Big) \quad (22)$$

is yielded where $i(k;I,Q)$ denotes the corresponding offsets for both in–phase and quadrature components, respectively. Note also that (22) implies $r_I[n] = \sum_{i=-\infty}^{\infty} \alpha_u \,\mathrm{sinc}\,(n - Ki - K + 1)\cos(\psi_m[i])$ and $r_Q[n] = \sum_{i=-\infty}^{\infty} \alpha_v \,\mathrm{sinc}\,(n - Ki)\sin(\varphi_m[i])$. Therefore:

$$\begin{aligned} R_{r_I}[k] &= E\{r_I[n] r_I[n+k]\} \\ &= \sum_{i=-\infty}^{\infty} \alpha_u \,\mathrm{sinc}\,(n - Ki - K + 1)\cos(\psi_m[i]) \times \\ &\sum_{v=-\infty}^{\infty} \alpha_u \,\mathrm{sinc}\,(n + k - Kv - K + 1)\cos(\psi_m[v]) \end{aligned} \quad (23)$$

is yielded. After some algebraic manipulations, one could reach:

$$\begin{aligned} R_{r_I}[k] &= E\{r_I[n] r_I[n+k]\} \\ &= \frac{1}{2}\alpha_u^2 \sum_{i=-\infty}^{\infty} \sum_{v=-\infty}^{\infty} \mathrm{sinc}\,(n - Ki - K + 1) \times \\ &\cdot \mathrm{sinc}\,(n + k - Kv - K + 1)\cos(2\pi f_\psi k) \end{aligned} \quad (24)$$



This work is licensed under a Creative Commons Attribution 4.0 License. For more information, see https://creativecommons.org/licenses/by/4.0/

This article has been accepted for publication in IEEE Access. This is the author's version which has not been fully edited and
content may change prior to final publication. Citation information: DOI 10.1109/ACCESS.2022.3195040



Note that in (24), Gibbs phenomenon is observed due to the finite support; however, its manifestation is controlled by $f_\psi$, which includes contributions of baseband message signal and presumably phase jitter in fading scenarios in case $\alpha_{u,v} \in \mathbb{R}$. In this regard, divergent $f_\psi$ dominates $R_{r_I}[k]$ and Gibbs phenomenon vanishes; whereas Gibbs phenomenon becomes clearer for convergent $f_\psi$. From the practical point of view, when $f_\psi$ solely includes the channel contribution and takes analytically the form of Jakes' model, $R_{r_I}[k] \approx J_0\left(2\pi f^D_{\text{norm}} k\right)$, where $f^D_{\text{norm}}$ denotes the normalized Doppler frequency related to (8). Therefore, by exploiting the approximation given in [29], $R_{r_I}[k]$ could be re-written as:

$$R_{r_I,r_Q}[k] = \frac{1}{2}\alpha^2_{u,v} \sum_{i=0}^{M-1} \frac{1}{2i-1} \times \cdot \sin\left(\frac{2\pi(2Ki - K + 1)k}{N}\right) \cos\left(2\pi f_\psi k\right) \tag{25}$$

where $N$ denotes the sampling rate for the buffer. At this point, it is desirable to demonstrate how channel affects the method proposed. In this sense, considering its statistical simplifications, let Jakes' model ($f_\psi \to 0$) be employed. Then, in light of (25), (21) could be rewritten as:

$$R_{\hat{\theta}}[k > 0] = 2\alpha^2_{u,v}\kappa^2\left(1 - \varrho\right) R_{r_{I,Q}}[k] \mathrm{D}^2\left\{R_{r_{I,Q}}[k]\right\} \tag{26}$$

or in expanded form:

$$R_{\hat{\theta}}[k > 0] = \frac{\alpha^2_{u,v}\kappa^2\left(1 - \varrho\right)\pi^2}{N^2} \sum_{i=0}^{M-1}\sum_{u=0}^{M-1} \frac{2i-1}{2u-1} \times \cdot \sin\left(\frac{2\pi(2i-1)k}{N}\right) \sin\left(\frac{2\pi(2u-1)k}{N}\right) \tag{27}$$

Finally, one could conclude that there exists $\varrho$ value which minimizes the difference between $R_{\hat{\theta}}[k > 0]$ and $R_{\theta}[k > 0]$ in the mean–square sense under the ambient channel characteristics. Optimal selection of $\varrho$ poses another research problem, which is outside the scope of this study. Therefore, numerical simulations will be employed to estimate the optimal value for $\varrho$ in here.

## IV. IMPLEMENTATION

This section discusses the details of the implementation of the proposed method. In order to provide a comprehensive perspective, the section initially briefs on a weather satellite as a real world signal source. Then, following the layout given in Figure 1, implementation of the antenna; technical details and relevant specifications of the software–defined radio (SDR) used; and finally the architecture of DSP along with required configuration structure are provided, respectively.

### A. WEATHER SATELLITE – NOAA-19

The National Oceanic and Atmospheric Administration – N Prime (NOAA-19) was launched into its orbit on February 6, 2009. Main purpose of NOAA-19 is to observe Earth and collect measurement data in various contexts some of which include radiation, atmospheric ozone level, sea surface temperature, and water profiles [30]. In this study, NOAA-19 is considered for various reasons:

- First of all, transmission could be considered to be line–of–sight (LOS) and the received signal is PM, which provides a suitable real world scenario to test the proposed design.
- Second, the transmission protocol is open and message data is multi–mode where an image (consisting of both regular/visible and infra–red segments) is always accompanied by several types of telemetry data. This way, both numerical and perceptual assessments could be established together.
- Third, in case a good reception opportunity (*i.e.*, appropriate weather conditions, orbital track match with the measurement location, and relatively lower interference temperature) is obtained, information broadcast includes measurement data relevant to the physical location where the measurement takes place.

NOAA-19 employs automatic picture transmission (APT) protocol mode and operates at 137.1MHz. A regular NOAA-19 transmission consists of a mixed mode multi–media stream which contains both near-real-time images taken by the satellite along with several pilot/synchronization signals and telemetry data. Once the stream is decoded successfully, two distinct images (visible and infrared) are expected to tile the frame side by side. Synchronization and telemetry data delineate images as the columns of tiles. In the stream, a single line includes 2080 pixels. Each image takes 909 pixels per single line. The remaining 262 pixels are reserved for telemetry and synchronization. Transmission rate is two lines per second. The stream consists of 256-level amplitude modulated baseband data impinged on a 2400 Hz subcarrier. The amplitude modulated subcarrier is then frequency modulated onto the actual transmission carrier operating at 137.1 MHz-band spreading across 38 kHz in the radio frequency (RF) spectrum. The signal emitted by NOAA-19 carries approximately 37 dB (5 W) effective radiated power [30]. Major parameters of NOAA-19 transmission are tabulated in Table 1.

**Table 1.** NOAA-19 Signal Characteristics

| | NOAA-19 |
|---|---|
| Physical layer signal | Frequency modulation with amplitude modulated subcarrier |
| Operation Frequency | 137.1MHz |
| Mode | automatic picture transmission |
| Modulation | AM 2400Hz subcarrier, 137.1MHz FM carrier |
| Bandwidth | 38kHz |
| Orbit | Polar |



This work is licensed under a Creative Commons Attribution 4.0 License. For more information, see https://creativecommons.org/licenses/by/4.0/

This article has been accepted for publication in IEEE Access. This is the author's version which has not been fully edited and
content may change prior to final publication. Citation information: DOI 10.1109/ACCESS.2022.3195040



### B. ANTENNA

Considering cost, portability of the measurement setup, and direction of arrival ambiguity during the capture, double cross antenna (DCA) Hence, in this study, a DCA is built and used to capture the satellite transmission.

The DCA design used in the measurements includes two orthogonal dipole pairs. Dipoles consist of copper wires of $2\,\mathrm{mm}$ radius and each dipole is assembled to the dielectric material end. Because NOAA-19 operates at $137.1\,\mathrm{MHz}$, antenna size requirements are driven by the wavelength of signal which is $\lambda \approxeq 2.2\mathrm{m}$. Therefore, dimensions of the antenna are given by $0.5\lambda = 1.1\mathrm{m}$, $0.25\lambda = 0.55\mathrm{m}$. Dipoles are indexed with $1, 2, 3,$ and $4$. Each dipole is of half–$\lambda$ length and is in–phase with the one across. In order to satisfy the polarization requirements, pairs $1-3$ and $2-4$ should carry a phase offset of $\pi/2$ where inter–dipole deviation angle is $\pi/6$ from the main axis. Planar view of the design is given in Figure 3 (side view of the antennae could be seen in Figure 5). Note that this phase offset should be compensated for before the signal processing stages take place. In this study, impact of phase offset is planned to be alleviated by keeping the $2-4$ cable pair larger than $1-3$ cable pair. Each cable is of RG58 C/U $50\,\Omega$ co-axial type. In the design, dielectric materials are of $55\,\mathrm{cm}$ long. The height of the antenna is $2\,\mathrm{m}$ considering the local measurement campaign requirements; however, longer antenna heights are desired to minimize surface reflection.

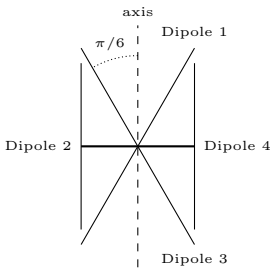


**Figure 3.** Planar view of dipoles. Note that side view of the antennae orientation is given Figure 5.

It is important to note further design parameters from practical point of view. Propagation speed of the signal within cables is an important design parameter since phase offset is planned to be calibrated by keeping one side longer. Based on the manufacturing specifications, RG58 C/U $50\,\Omega$ co-axial cable delays the signal by $\frac{1}{3}c$ leading to a relative transmission speed of $\approxeq 0.66c$, where $c$ is the speed of light. Considering both reception and phase compensation concerns, lengths of the dipole pairs are chosen to be $\lambda$ and $\lambda + 0.25\lambda$, yielding $\approxeq 1.44\mathrm{m}$ and $\approxeq 1.80\mathrm{m}$, respectively.

The final step of the antenna setup is to hook up the design with the SDR platform. In order to have a sturdy connection, shield of each cable is connected with its pair; core of the first cable is soldered with the second and that of the third cable is soldered with the fourth. Output terminal contains solely the cores of co-axial cables. Cores of first and second cables are connected to the shield of output terminal, whereas those of third and fourth cables are connected to the core of output terminal. A single dipole structure is given in Figure 4 with the corresponding dimensions. Finally, a $50\,\Omega$ SMA connector is assembled to the end of output terminal to connect DCA to SDR by meeting impedance matching requirements.

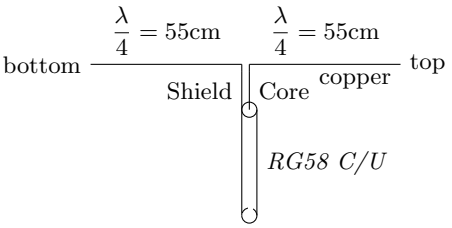


**Figure 4.** Structure of a single dipole.

### C. SDR

The chipset that is used on SDR is known to be RTL-SDR. It employs Realtek's RTL2832 Demodulator IC and R280T2 "High Performance Low Power Advanced Digital TV Silicon Tuner" chips. These chipsets enable the NooElec NESDR SMArt RTL-SDR to operate from $25\,\mathrm{MHz}$ to $1700\,\mathrm{MHz}$. Thanks to up-converter and down-converter devices, the operation range of RTL-SDR can be expanded to a certain extent. NESDR SMArt RTL-SDR can communicate with computer through the use of universal serial bus (USB) 2.0 or USB 3.0 protocols with the maximum transfer rate of $480$Msps [31].

### D. DSP IMPLEMENTATION

Fractionally sub–Nyquist receiver is implemented on both MATLAB and ANSI-C. Note that ANSI-C implementation is designed in such a way that the proposed method can run on an ARM–based microcontroller (Cortex-M4-based STM32F4 series) with DSP instructions on Q1.31 format under direct memory access (DMA) support [32]. Because there is no graphical user interface of microcontroller, once the data processing is done, output is transferred onto a personal computer for further processing and display purposes via the tools such as OpenOCD and GDB (with appropriate ARM EABI) in order to verify the results. Hence, MATLAB is used for high–level implementation of the proposed method, searching for the optimal value of the autoregressive process and numerical evaluations, verification of the microcontroller output to compare the results, and display.

Before proceeding with the field measurements and corresponding results, it is appropriate here first to discuss the impact of fractionally asymmetric sub–Nyquist receiver on the phase estimation, which is critical for PM signals. Without loss of generality, the message signal, $m(t)$, is selected to be a pure tone with unity power in the low–pass



This work is licensed under a Creative Commons Attribution 4.0 License. For more information, see https://creativecommons.org/licenses/by/4.0/

This article has been accepted for publication in IEEE Access. This is the author's version which has not been fully edited and
content may change prior to final publication. Citation information: DOI 10.1109/ACCESS.2022.3195040



region and impinged on a carrier signal via FM with the commercial FM configurations. Transmit signal is passed through propagation channel with various configurations. Transmission chain is completed with the addition of white noise. At the receiver side, output of several sub–Nyquist versions of various rates are fed into the phase estimator where estimator output is scaled into unity power so that a fair comparison could be established.

## V. REAL-WORLD DATA COLLECTION

Measurement data are collected in different times and places due to the orbital track of the satellite. Considering the measurement campaign parameters such as weather conditions, orbital track match with the measurement location, and interference temperature in the vicinity of measurement location, only the best (*i.e.*, highest signal–to–noise ratio (SNR), minimum interference temperature, clear sky, open area without high–rise buildings around, widest footprint, etc.) data are used in the post–processing stages. Among many measurement campaigns, only two sets meet the requirements mentioned here in a partial manner (cloudy rather than being clear sky), whose parameters are given in Table 2. During each and every measurement session, smartphone applications which allow one to track orbits of satellites, planets, stars with the aid of its compass and gyroscope sensors accompany the footprint and measurement campaign along with the antenna orientation. SDR plug-ins are employed to check with the instantaneous quality of the reception. An instant from measurement preparation for an expected satellite pass is given in Figure 5.

**Table 2.** Recording Parameters

| Date | Location | Weather | Duration | Q. of Pass |
|---|---|---|---|---|
| Nov. 27$^{\text{th}}$, 2018 | 40–57'10.7"N 29–07'09.1Ë | Cloudy | 699s | 75% |
| Nov. 28$^{\text{th}}$, 2018 | 40–56'27.4"N 29–06'06.9Ë | Cloudy | 661s | 86% |

## VI. RESULTS AND DISCUSSIONS

The proposed method is run after feeding the captured field measurement data into the receiver. The receiver functions in two modes. In the first mode, regular NOAA-19 receiver operates directly on the captured data and decodes the image that is transferred by the satellite as a PM signal. In the second mode, several values defining the fractionally sub-Nyquist receiver are selected to drive the receiver and corresponding image output set is obtained.

One of the key points in evaluating the performance of the method proposed is to obtain autoregressive coefficient, $\varrho$, for $K = 2, \Delta = 1$, which minimizes the error. In order to investigate the impact of channel, first, both frequency–flat and selective fading channels are employed in high–SNR regime. Figure 6 includes the ITU-R M.1225 Vehicular Channel A configuration with classical Jakes' Doppler spectrum where each tap is Rayleigh distributed and SNR is 20dB. As described in Section III, the proposed method exploits the channel characteristics when there are multiple resolvable multipath components and could achieve mean–squared–error (MSE) levels on the order of $-20$dB or even below, whereas its performance almost never improves for flat–fading scenario. This behavior is a direct consequence of (14) and (26) since the proposed method could easily capture the statistical variations in the frequency–selective fading scenario; however, flat–fading scenario does not provide sufficient temporal diversity for the proposed method to improve its performance.

Performance of the proposed method is investigated with a different tap gain distribution is given in Figure 7. In Figure 7, the ITU-R M.1225 Vehicular Channel A configuration of classical Jakes' Doppler spectrum is again employed to establish a fair comparison with the results in Figure 6. However, in Figure 7, each tap is Rician distributed with $K$–factor of 3. It is important to note here that performance under Rician distribution is critical since real world measurements include a link between a satellite and a ground station (the proposed receiver). In comparison with the results presented in Figure 6, one could conclude that flat–fading behavior is slightly worse than that in Rayleigh distributed scenario even though the overall behavior is almost identical. On the other hand, impact of channel correlation becomes more apparent for the proposed method in Rician fading under frequency–selective scenarios. This stems from the fact that channel correlation does not decay as fast as that in Rayleigh fading scenario for diverging $K$–factor. Note that this is a direct consequence of the fact that autoregressive process (with $\varrho$ value obtained through the use of simulation) expects a relatively faster drop due to its exponential decay nature. Nevertheless, both fading configurations lead to very close autoregressive coefficient values for the offset $K = 2$.

Once the autoregressive coefficient is obtained, MSE behavior of the proposed method for various sub–Nyquist offsets under different SNR regimes could be investigated. Figure 8 includes the MSE behavior of the proposed method for several configurations. As can be seen in Figure 8, as sub–Nyquist rate increases, MSE performance deteriorates. Furthermore, sub–Nyquist offset $K = 2$ manifests some sort of an exponential improvement as SNR increases, whereas $K > 2$ cases exhibit almost no improvement as SNR improves. This phenomenon relies heavily on the amount of –especially phase– information lost. When (13) is analyzed in detail, impact of $K$ could be seen in a better way. As $K$ increases in (13) the coefficients of harmonics would be less pronounced due to the $\mathrm{sinc}(\cdot)$ driven both by the presence of constant anti–alias filter bandwidth $B$ and an increasing $K$.

At this point, it is worth discussing the results of comparison between different sub–Nyquist receivers. Figure 9 provides the comparison results of two different sub–Nyquist receivers and our proposed design: The first receiver is the



This work is licensed under a Creative Commons Attribution 4.0 License. For more information, see https://creativecommons.org/licenses/by/4.0/

This article has been accepted for publication in IEEE Access. This is the author's version which has not been fully edited and
content may change prior to final publication. Citation information: DOI 10.1109/ACCESS.2022.3195040



standard uniform sampling (no offset, *i.e*, $\Delta = 0$) sub–Nyquist receiver with $K = 2$, whereas the second one is the random sampling sub–Nyquist receiver with effective value of $K = 2$ and $\Delta = 0$. The effective value of $K = 2$ for random sampling receiver is achieved by flipping a valid, fair coin to decide whether the next sample will be taken. In order to achieve a fair comparison between receiver performances, an AWGN channel of low SNR regime, namely 10dB, is adopted and error performances are obtained with the aforementioned settings and configurations for a short period of time window. First of all, it is clear that error performance of the proposed method yields better results as compared to those of other methods. This is not unexpected since standard uniform sampling and random sampling sub–Nyquist receivers cannot keep up with the phase transitions as well as the proposed method taking advantage of $\Delta = 1$. For the sake of completeness, one should note that random sampling receiver achieves worse performance compared to that of standard uniform sampling sub–Nyquist receiver. This is expected since random sampling could capture consecutive samples occasionally ($K = 1$ case) to achieve the lowest error performance; on the other hand, magnitudes of errors would be slightly higher for $2 < K$ cases.

Before proceeding with the real world results, one could discuss the performance of the method proposed under more sophisticated propagation channel mechanisms such as multimodal Doppler behavior along with doubly selective characteristics. In such cases, the proposed method could still survive to some extent since the statistical behavior of the channel could still be captured with the aid of (presumably a higher order) autoregressive process given in (14). On the other hand, model parameter selection requires a careful analysis and their on–the–fly computations might not be feasible. Thus, it would be wiser to obtain pre-computed models along with their parameters based on the statistical propagation channel model classes available for the receiver of interest.

The proposed model is tested in a real–world communication scenario including all sorts of impairments and imperfections as well. In order to highlight performance of the receiver, first, Nyquist–rate receiver is run and its output is obtained. The results for the shorter data captured (with higher quality of pass) are given in Figure 10 along with several key points. As can be seen, data transmitted with the use of PM consist of several parts including pilot symbols and some measurement results beside images (both regular/visible and infra–red side by side). It is important to note that each pass, as described in Table 2, is different from another in several perspectives such as the quality of pass, footprint, weather conditions, and RF front–end operating considerations such as ambient interference temperature. Hence, Figure 10 will be used as a reference for performance comparison of output of the proposed receiver.

One of the main purposes of fractionally asymmetric sub–Nyquist receiver is to reduce the bandwidth requirements of the receiver while maintaining important characteristics of the transmit signal. In this sense, halving the bandwidth is a critical threshold. Figure 11 demonstrates the impact of halving the bandwidth for the receiver. There are two major discernible effects present in comparison with Figure 10: A more emphasized stripe pattern (which already exists in the ideal receiver output to some extent) and increase in the ambiguity in the lower part of the figure covering the telemetry data. However, halving the bandwidth does not affect the pilot estimation at all, as can be seen from the left–most column of Figure 11.

Once the impact of halving the fractionally sub–Nyquist receiver is observed, it is natural to extend it to a further decrease in bandwidth. Figure 12 shows the results when one–third of the bandwidth is evaluated. As can be seen from the figure, the degradation in the lower part of the image becomes evident. However, one should pay attention to the fact that the pilots could still be identified sufficiently accurate in this scenario.

As discussed in the previous cases, a dramatic degradation starts when pilots could not be estimated accurate enough. This could be seen in Figure 13 where the proposed receiver operates in one–fourth of the bandwidth. The following points could be observed based on the results: First, some of the pilots are not estimated, whereas some of them are completely missed. Consequently, corresponding lines are smothered by the ambient noise. Second, some of the pilots are estimated in an erroneous way, which is the natural result of dramatic phase mismatch stemming from the linear interpolation employed in this study. Third, the overall phase interpolation fails dramatically such that infra–red portion of the image is totally swamped out.

## VII. CONCLUSION AND FUTURE WORKS

In this study, a fractionally asymmetric sub–Nyquist receiver is designed, implemented, and tested in a real–world reception scenario through the use of an active weather satellite transmit signal. The receiver benefits from the stationarity of the channel characteristics in such a way that phase changes are captured with the use of first–order autoregressive process in a predictive manner while operating at sub–Nyquist region. Field measurements reveal that the proposed receiver could still provide sufficient fidelity and/or quality for the PM signals where the receiver operates within half of the bandwidth. As can be seen, phase information that is missed due to sub–Nyquist sampling could still be recovered by the autoregressive process to some extent.

This study reveals that sub–Nyquist receivers could be extended in various ways. First of all, optimal selection strategy for autoregressive coefficient could be investigated so that an analytic expression could be devised for certain channel configurations. Second, fractional asymmetry could be generalized in such a way that discrete multi-coset approach covers also the scenarios where $K \in \mathbb{Q}$. Finally, the performance analysis of the sub–Nyquist receivers could be carried out for signals whose envelope variations are relatively higher.



This work is licensed under a Creative Commons Attribution 4.0 License. For more information, see https://creativecommons.org/licenses/by/4.0/

This article has been accepted for publication in IEEE Access. This is the author's version which has not been fully edited and
content may change prior to final publication. Citation information: DOI 10.1109/ACCESS.2022.3195040



## References

[1] CISCO, "Cisco Annual Internet Report (2018–2023)," CISCO, USA, White Paper, Mar. 2018, updated on Mar. 9, '20.

[2] J. A. Stankovic, "Research directions for the internet of things," IEEE Internet of Things Journal, vol. 1, no. 1, pp. 3–9, 2014.

[3] J. Jin, J. Gubbi, S. Marusic, and M. Palaniswami, "An information framework for creating a smart city through internet of things," IEEE IoT Jnl., vol. 1, no. 2, pp. 112–121, 2014.

[4] K. Boriboonsomsin, M. J. Barth, W. Zhu, and A. Vu, "Eco-routing navigation system based on multisource historical and real-time traffic information," IEEE Trans. on Intel. Trans. Sys., vol. 13, no. 4, pp. 1694–1704, 2012.

[5] P. M. d'Orey and M. Ferreira, "ITS for sustainable mobility: A survey on applications and impact assessment tools," IEEE Trans. on Intel. Transp. Sys., vol. 15, no. 2, pp. 477–493, 2014.

[6] L. Mohjazi, A. Zoha, L. Bariah, S. Muhaidat, P. C. Sofotasios, M. A. Imran, and O. A. Dobre, "An outlook on the interplay of artificial intelligence and software-defined metasurfaces: An overview of opportunities and limitations," IEEE Vehicular Technology Magazine, vol. 15, no. 4, pp. 62–73, 2020.

[7] Y. Hur, J. Park, W. Woo, J. S. Lee, K. Lim, C.-H. Lee, H. S. Kim, and J. Laskar, "A Cognitive Radio (CR) System Employing A Dual-Stage Spectrum Sensing Technique: A Multi-Resolution Spectrum Sensing (MRSS) and A Temporal Signature Detection (TSD) Technique," in IEEE Global Telecomm. Conf., CL, USA, Nov. 2006, pp. 1–5.

[8] W.-Y. Lee and I. F. Akyildiz, "Optimal spectrum sensing framework for cognitive radio networks," IEEE Trans. on Wireless Comm., vol. 7, no. 10, pp. 3845–3857, Oct. 2008.

[9] J. A. Tropp, J. N. Laska, M. F. Duarte, J. K. Romberg, and R. G. Baraniuk, "Beyond nyquist: Efficient sampling of sparse bandlimited signals," IEEE Transactions on Information Theory, vol. 56, no. 1, pp. 520–544, 2010.

[10] C. R. Berger, Z. Wang, J. Huang, and S. Zhou, "Application of compressive sensing to sparse channel estimation," IEEE Communications Magazine, vol. 48, no. 11, pp. 164–174, 2010.

[11] X. Chen, Z. Yu, S. Hoyos, B. M. Sadler, and J. Silva-Martinez, "A sub-nyquist rate sampling receiver exploiting compressive sensing," IEEE Transactions on Circuits and Systems I: Regular Papers, vol. 58, no. 3, pp. 507–520, 2011.

[12] M. Torlak and W. Namgoong, "Sub-nyquist sampling receiver for overlay cognitive radio users," IEEE Transactions on Signal Processing, vol. 66, no. 16, pp. 4160–4169, 2018.

[13] K. V. Mishra, Y. C. Eldar, E. Shoshan, M. Namer, and M. Meltsin, "A cognitive sub-nyquist mimo radar prototype," IEEE Transactions on Aerospace and Electronic Systems, vol. 56, no. 2, pp. 937–955, 2020.

[14] C. Cui, W. Wu, and W.-Q. Wang, "Carrier frequency and doa estimation of sub-nyquist sampling multi-band sensor signals," IEEE Sensors Journal, vol. 17, no. 22, pp. 7470–7478, 2017.

[15] E. Candès and J. Romberg, "Sparsity and incoherence in compressive sampling," Inverse Problems, vol. 23, no. 3, p. 969–985, Apr. 2007.

[16] R. G. Baraniuk, "Compressive sensing [lecture notes]," IEEE Signal Processing Magazine, vol. 24, no. 4, pp. 118–121, 2007.

[17] E. Candes and M. Wakin, "An introduction to compressive sampling," IEEE Sig. Pro. Mg., vol. 25, no. 2, pp. 21–30, 2008.

[18] D. L. Donoho, "Compressed sensing," IEEE Trans. on Info. Theo., vol. 52, no. 4, pp. 1289–1306, 2006.

[19] M. Verhelst and A. Bahai, "Where analog meets digital: Analog–to–information conversion and beyond," IEEE Solid-state circuits magazine, vol. 7, no. 3, pp. 67–80, 2015.

[20] X. Chen, E. A. Sobhy, Z. Yu, S. Hoyos, J. Silva-Martinez, S. Palermo, and B. M. Sadler, "A sub-nyquist rate compressive sensing data acquisition front-end," IEEE Jnl. on Emerging and Sel. Top. in Circ. & Syst., vol. 2, no. 3, pp. 542–551, 2012.

[21] P. Daponte, L. De Vito, S. Rapuano, and I. Tudosa, "Analog-to-information converters in the wideband rf measurement for aerospace applications: current situation and perspectives," IEEE Instr. Meas. Mag., vol. 20, no. 1, pp. 20–28, 2017.

[22] M. R. Chowdhury, S. Tripathi, and S. De, "Adaptive multivariate data compression in smart metering internet of things," IEEE Trans. on Ind. Info., vol. 17, no. 2, pp. 1287–1297, 2021.

[23] J. Marecek, S. Maroulis, V. Kalogeraki, and D. Gunopoulos, "Low-rank methods in event detection with subsampled point-to-subspace proximity tests," IEEE Access, pp. 1–1, 2022.

[24] Yiyuan Xiong, Yi Huang, J. F. Ralph, W. Al-Nuaimy, and Pu Sun, "An fm demodulation algorithm with an undersampling rate," in Proc. IEEE Intnl. Conf. on Acoustics, Speech, and Signal Processing, vol. 6, 2003, pp. VI–245.

[25] J. Dong, H. Li, Z. Fan, Q. Zhou, and S. Hua, "A joint optimization algorithm using adaptive minimum coset number based discrete multi-coset sampling," IEEE Access, vol. 8, pp. 168 659–168 670, 2020.

[26] Y. Xiong, Y. Huang, J. Ralph, W. Al-Nuaimy, and P. Sun, "An fm demodulation algorithm with an undersampling rate," in 2003 IEEE International Conference on Acoustics, Speech, and Signal Processing, 2003. Proceedings. (ICASSP '03)., vol. 6, 2003, pp. VI–245.

[27] E. Candes, J. Romberg, and T. Tao, "Stable signal recovery from incomplete and inaccurate measurements," 2005.

[28] E. Candes and T. Tao, "Decoding by linear programming," IEEE Transactions on Information Theory, vol. 51, no. 12, pp. 4203–4215, 2005.

[29] A. E. Karatsuba, "Calculation of bessel functions via the summation of series," Numerical Analysis and Applications, vol. 12, no. 4, pp. 372–387, 2019.

[30] J. Robel and A. Graumann, "NOAA KLM user's guide with NOAA-N, n prime, and MetOp supplements," National Oceanic and Atmospheric Administration National Environmental Satellite, Data, and Information Service National Climatic Data Center Remote Sensing and Applications Division, pp. 1–2530, aug 2014.

[31] Nooelec, "Nooelec—Nooelec NESDR SMArt SDR—Premium RTL-SDR w/Aluminum Enclosure, 0.5PPM TCXO, SMA Input. RTL2832U & R820T2-Based—Software Defined Radio." 2017, last accessed 4 June 2022. [Online]. Available: https://www.nooelec.com/store/sdr/nesdr-smart-sdr.html

[32] STM, "Reference manual for STM32F405-415, STM32F407-417, STM32F427-437 and STM32F429-439 advanced Arm-based 32-bit MCUs," 2019, last accessed 4 June 2022. [Online]. Available: https://www.st.com/resource/en/reference_manual/rm0090-stm32f405415-stm32f407417-stm32f427437-and-stm32f429439-advanced-armbased-32bit-mcus-stmicroelectronics.pdf



This work is licensed under a Creative Commons Attribution 4.0 License. For more information, see https://creativecommons.org/licenses/by/4.0/

This article has been accepted for publication in IEEE Access. This is the author's version which has not been fully edited and
content may change prior to final publication. Citation information: DOI 10.1109/ACCESS.2022.3195040



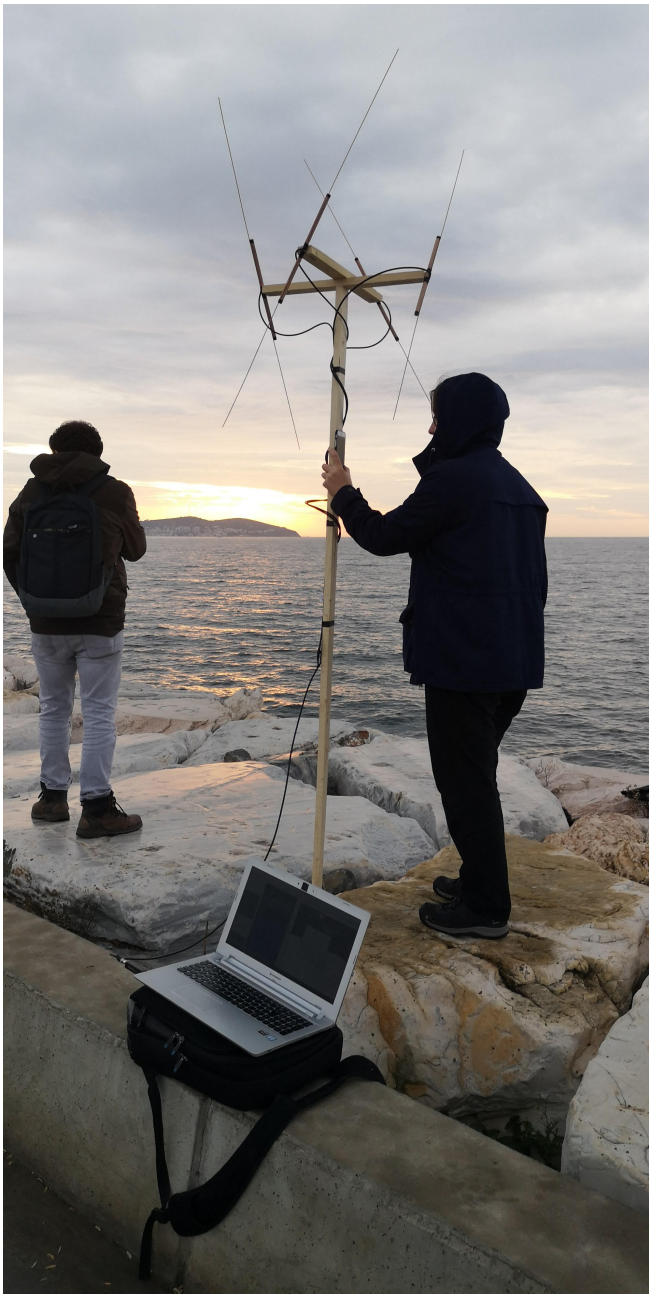

**Figure 5.** Picture of the antenna designed and its connection to computer via SDR. Team (Tapir Lab.) members are seen as trying to decide the location of the antenna and setup before the pass.

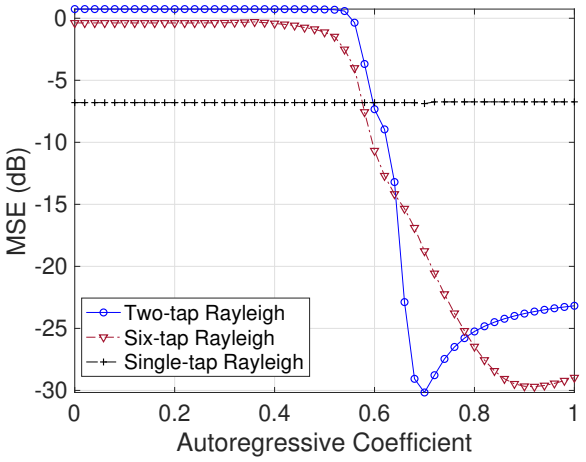


**Figure 6.** MSE performance of the proposed method with $K = 2, \Delta = 1$ under several Rayleigh channel configurations.

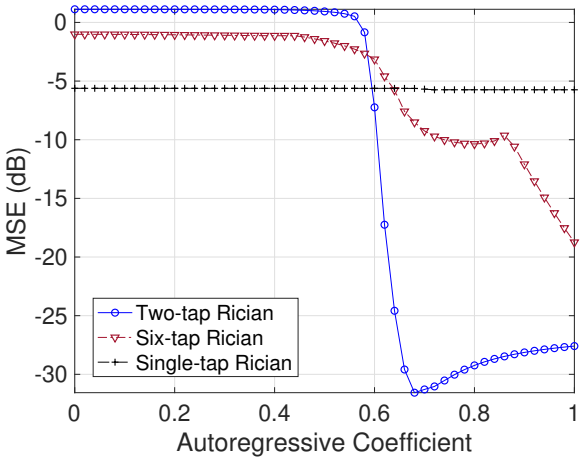


**Figure 7.** MSE performance of the proposed method with $K = 2, \Delta = 1$ under several Rician channel configurations.

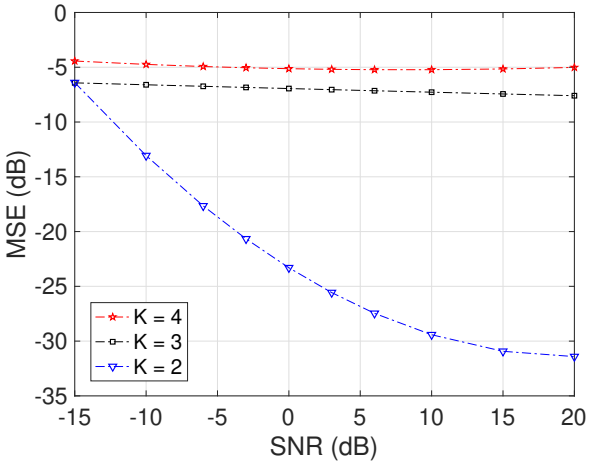


**Figure 8.** Mean–square–error behavior of the proposed method with different offsets ($\Delta = 1$) under various SNR levels.



This work is licensed under a Creative Commons Attribution 4.0 License. For more information, see https://creativecommons.org/licenses/by/4.0/

This article has been accepted for publication in IEEE Access. This is the author's version which has not been fully edited and
content may change prior to final publication. Citation information: DOI 10.1109/ACCESS.2022.3195040



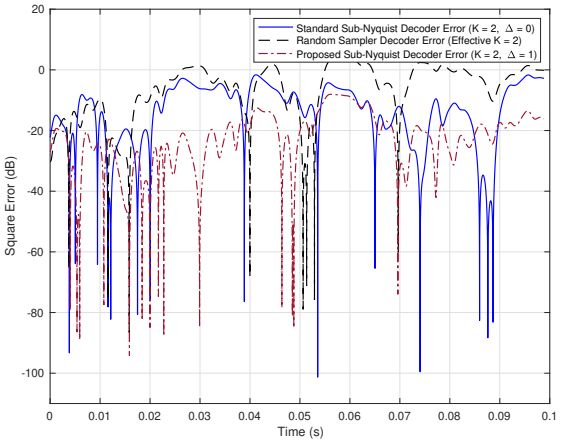


**Figure 9.** Error performance comparison of several sub–Nyquist receivers along with that of the proposed method.

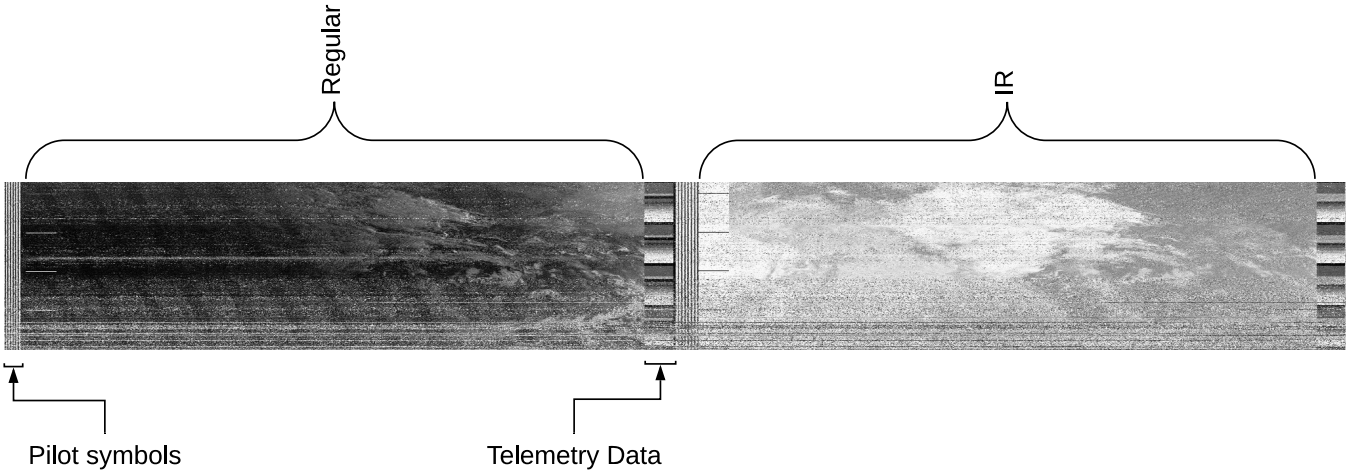


**Figure 10.** Nyquist rate receiver output along with several pieces of information provided in the data.

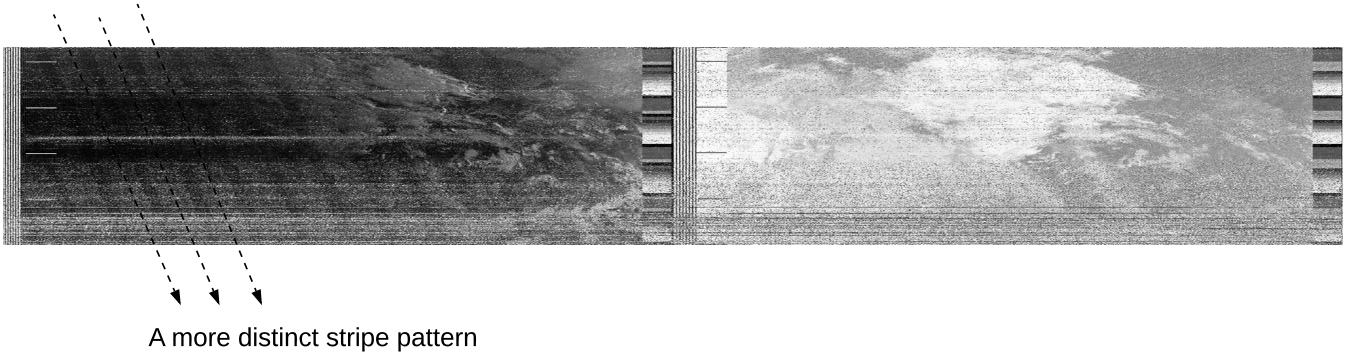


**Figure 11.** Fractionally sub–Nyquist (by $K = 2, \Delta = 1$, halving the bandwidth) receiver output. Note the more distinct stripe pattern along with increased ambiguity in the lower part of the image.



This work is licensed under a Creative Commons Attribution 4.0 License. For more information, see https://creativecommons.org/licenses/by/4.0/

This article has been accepted for publication in IEEE Access. This is the author's version which has not been fully edited and
content may change prior to final publication. Citation information: DOI 10.1109/ACCESS.2022.3195040



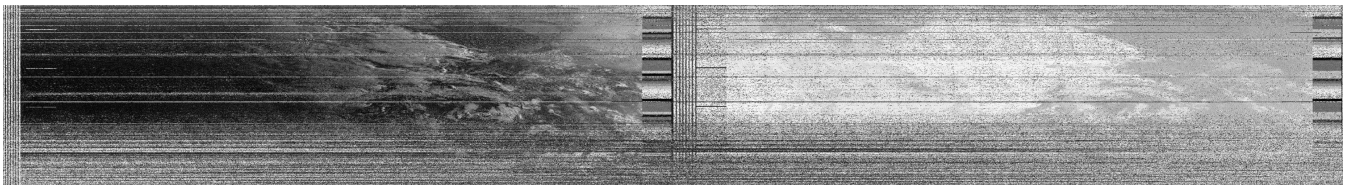

**Figure 12.** Fractionally sub–Nyquist (by $K = 3, \Delta = 1$, one–third of the bandwidth) receiver output.

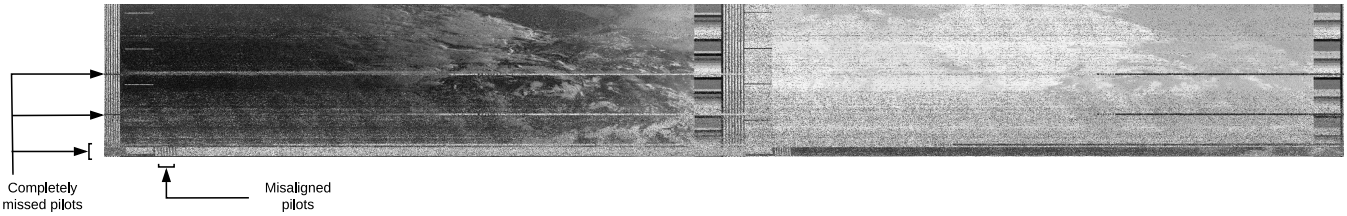


**Figure 13.** Fractionally sub–Nyquist ($K = 4, \Delta = 1$, quarter of the bandwidth) receiver output.



This work is licensed under a Creative Commons Attribution 4.0 License. For more information, see https://creativecommons.org/licenses/by/4.0/

This article has been accepted for publication in IEEE Access. This is the author's version which has not been fully edited and
content may change prior to final publication. Citation information: DOI 10.1109/ACCESS.2022.3195040





ZEYNEP GÜRKAŞ-AYDIN received her BSc and MSc in Computer Engineering from Istanbul University. In 2011 and 2014, she received PhD degrees in computer engineering from Istanbul University and computer science from Université Pierre-Et-Marie-Curie: Paris VI / Telecom SudParis. Her current areas of expertise include data and computer communications, wireless and mobile networks, the internet of things, and cyber security. She is currently an Assistant Professor in the Department of Computer Engineering Cyber Security Department at Istanbul University in Istanbul, Turkey. She is also a member of Istanbul University-Cerrahpasa's Internet of Things Security Test and Evaluation Center (ISTEC). Additionally, her current research interests are about indoor localization, internet of things, cyber security, complex network analysis and communication networks.



SERHAN YARKAN received the B.S. and M.Sc. degrees in computer science from Istanbul University, Istanbul, Turkey, in 2001 and 2003, respectively, and the Ph.D. degree from the University of South Florida, Tampa, FL, USA, in 2009. He was a Post-Doctoral Research Associate with the Department of Computer and Electrical Engineering, Texas A&M University, College Station, TX, USA, from 2010 to 2012. Currently, he is an Associate Professor in Electrical-Electronics Engineering at Istanbul Commerce University, Istanbul. Serhan Yarkan's current research interests include statistical signal processing, cognitive radio, wireless propagation channel measurement and modeling, cross-layer adaptation and optimization, and interference management in next-generation wireless networks, and underground mine channels and disaster communications.



This work is licensed under a Creative Commons Attribution 4.0 License. For more information, see https://creativecommons.org/licenses/by/4.0/